Catalysis Science & Technology

Accepted Manuscript

ROYAL SOCIETY OF CHEMISTRY

www.rsc.org/catalysis

Improved silica-titania catalysts by chitin bio-templating

Alexander Sachse,[a] Vasile Hulea,[a] Krassimir L. Kostov,[b] Emmanuel Belamie[a] and Bruno Alonso*[a]

[a] Institut Charles Gerhardt Montpellier -UMR 5253 CNRS/UM2/ENSCM/UM1, 8 rue de l'Ecole Normale, 34296 Montpellier Cedex 5, France. E-mail: bruno.alonso@enscm.fr

[b] Institute of General and Inorganic Chemistry, Bulgarian Academy of Sciences, Acad. G. Bonchev. Str., bl. 11, 1113 Sofia, Bulgaria.

Table of Content Entry

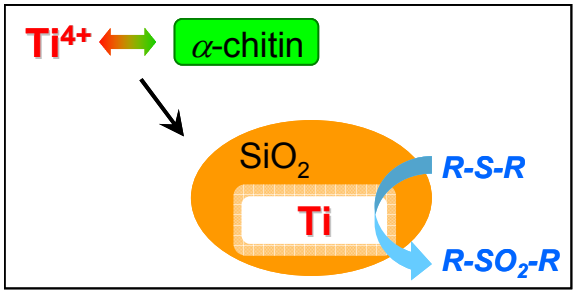

New silica-titania mesoporous catalysts with improved performances were achieved by combining surface and templating properties of α-chitin nanorods recovered from the biomass with sol-gel and spray-drying processes.

Improved silica-titania catalysts by chitin bio-templating

Alexander Sachse,[a] Vasile Hulea,[a] Krassimir L. Kostov,[b] Emmanuel Belamie[a] and Bruno Alonso*[a]

[a] Institut Charles Gerhardt Montpellier -UMR 5253 CNRS/UM2/ENSCM/UM1, 8 rue de l'Ecole Normale, 34296 Montpellier Cedex 5, France. E-mail: bruno.alonso@enscm.fr

[b] Institute of General and Inorganic Chemistry, Bulgarian Academy of Sciences, Acad. G. Bonchev. Str., bl. 11, 1113 Sofia, Bulgaria.

Table of Content Entry

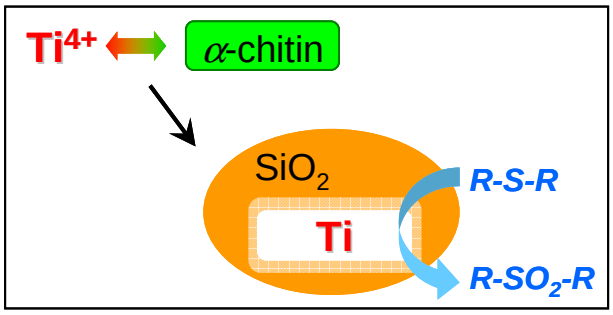

New silica-titania mesoporous catalysts with improved performances were achieved by combining surface and templating properties of α-chitin nanorods recovered from the biomass with sol-gel and spray-drying processes.

Abstract

Silica-titania materials with improved catalytic performances were elaborated as mesoporous microparticles by combining sol-gel and spray-drying processes with the self-assembly properties of α-chitin nanorods acting as bio-templates. Three different synthesis' approaches are discussed, leading to materials with varied textural and chemical characteristics studied by SEM, N_2 volumetry, TEM, XPS and DR-UV techniques. The use of water or ethanol as initial solvent for the chitin nanorods' suspensions, as well as the mixing conditions of the precursors show to have a significant impact on the final properties. Materials of specific surface areas of up to 590 $m^2.g^{-1}$ and porous volumes of up to 0.84 $mL.g^{-1}$, with low surface Si/Ti ratio could be disclosed. Properties were further investigated by employing the silica-titania materials as heterogeneous catalysts for the sulfoxidation of bulky model compounds. The location of Ti active sites at the pore surface has been maximized and allows for improved productivity.

1. Introduction

Very recently we have published a novel and green synthesis route, which implies the use of chitin-nanorods as templates for the achievement of very active mesoporous silica-titania catalysts.[1] This research has been motivated by the fact that promising alternatives for the formation of silica-titania catalysts are highly demanded especially from the petroleum and pharmaceutical industry.[2] Indeed, desulfurization with H_2O_2 by catalytic oxidation, using silica-titania catalysts is a valuable alternative for the elimination of sulfur containing compounds from fuels by conversion of sulfides into the corresponding sulfoxides and sulfones which can easily be extracted due to their increased polarity.[3-5] Furthermore catalytic sulfoxidation has attracted a great deal of attention for the production of fine chemicals.[6]

Several different silica-titania catalysts are known in the literature. The first ones to be disclosed were Ti containing zeolites as TS-1, TS-2 and Ti-beta which proved to be very active catalysts for a variety of oxidation reactions with H_2O_2.[7-10] Notwithstanding, these materials showed to have important drawbacks which are mainly related to the sole presence of micropores; limiting thus the accessibility of large molecules to active sites. As a result, much effort has been devoted to the synthesis of mesoporous amorphous TiO_2-SiO_2 mixed oxides. Strategies for the synthesis of these materials became available from the early 1990s.[11] Examples hereof are the direct synthesis of ordered mesoporous materials (e.g. Ti-MCM-41, Ti-MCM-48),[12-15] the grafting of Ti species onto mesoporous silicas[16,17] and both hydrolytic[18,19] and non-hydrolytic[20,21] sol-gel synthesis routes. Most of these materials proved to be active catalysts for oxidation reactions of larger molecules, especially with dry organic hydroperoxides, and not with H_2O_2. Another drawback of these materials is that their synthesis often relies on complex techniques (use of glove box, dry solvents, etc.) and in some cases, expensive template materials such as CTAB are employed. Other synthesis' approaches must then be explored.

Green chemistry is a general trend, mainly motivated by the desire to generate products by sustainable means.[22-23] Within this, alternative synthesis routes for the formation of heterogeneous catalysts by so-called green pathways are in the center of the attention.[24-27] Various research groups have published the achievement of porous materials by bio-inspired techniques[28-35] using self-assembled polysaccharide nano-crystals, in combination with sol-gel processes for the transcription of the textural properties in the new materials.[36-42]

A novel and versatile route for the formation of porous silicas has been described by some of us.[37,38] This approach combines the self assembly properties of α-chitin nanorods[43,44] with sol-gel processes involving siloxane oligomers. There are several advantages of applying this

strategy to the synthesis of mesoporous materials among which: a) the use of renewable chitin precursors coming from crustacean (shrimps, crabs, …) fisheries where crustacean shells amount as waste product in tremendous quantities, b) the use of α-chitin nanorods acting as hard templates (D = 23 ±3 nm, L = 260 ±80 nm) and also possessing complexing groups (-OH, -NH_2) at their deacetylated surface, c) the high modularity of the final pore textures relying in the self-assembly properties of α-chitin nanorods, d) the use of low temperature sol-gel processes; e) the flexibility of sol-gel processes allowing for shaping of the materials (i.e. microparticles through spray-drying) and for incorporating other elements.

More recently, we have shown that this combination of chitin self-assembly, sol-gel chemistry and spray-drying processes allows in obtaining new efficient silica-titania catalysts.[1] The use of spray-drying offers here other advantages:[45] a) all reactants are incorporated in the final microparticles, b) the waste solvent is recycled through an condensing unit, and c) the continuous production of materials with desired spheroidal morphology. An additional advantage of this technique is the quenching of metastable states by fast solvent evaporation and solidification, whilst offering opportunities to fine-tune the mesoporosity and chemical composition of the resulting solid.[46-48]

In this study, we widen the synthetic possibilities in order to improve the textural properties and catalytic performances of the obtained silica-titania mixed oxides. In particular, we tried to modulate the distribution of Ti sites at the pore surfaces by playing with the initial preparation of the sols, in view of a greener process intensification.

2. Results and discussion

Three different strategies were investigated for the elaboration of porous silica-titania catalysts, with the aim of reaching an improved control of colloidal and molecular interactions, and hence to achieve better defined interfaces and active site distributions. The first (series A), based on our preliminary communication,[1] is achieved by mixing an ethanolic sol of siloxane oligomers (~3 nm in size) with fixed amounts of the titanium monomer precursor diacetylacetonatediisopropoxide titanium (IV) $Ti(O^iPr)_2(acac)_2$. Subsequently, an aqueous suspension of α-chitin nanorods is added. To prevent uncontrolled condensation of the inorganic precursors, water is rapidly removed from the resulting mixture by repeated evaporation cycles near the water-ethanol azeotrope composition. The resulting ethanolic suspension is subsequently spray-dried at 393 K in order to obtain fine powders named SiO_2/TiO_2-A materials (**Scheme 1A**). In the second strategy (series B), the ethanolic mixture, containing $Ti(O^iPr)_2(acac)_2$ and siloxane oligomers, is added to α-chitin nanorods directly

suspended in ethanol. Since no water is present in this mixture, this stable suspension is directly spray-dried to give SiO_2/TiO_2-B materials (**Scheme 1B**). Finally, a third strategy (series C) was designed to favor interactions between the Ti units and the α-chitin nanorods surface, with the aim of enriching the pore surfaces with Ti active sites after chitin removal. To this purpose, $Ti(O^iPr)_2(acac)_2$ was first mixed with the ethanolic chitin suspension, and the suspension of siloxane oligomers added subsequently (**Scheme 1C**).

The α-chitin polysaccharide nanorods present in the hybrid materials are removed by calcination in air at 823 K, resulting in the creation of porosity. During this process, the inorganic network also condenses further. The textural parameters of the materials are greatly influenced by the amount of chitin added during the synthesis (expressed as the chitin volume fraction, $\phi_{CHI,}$, using **Eq. 1** in the Experimental Section).

2.1 Series A materials

Morphology

Spheroidal microparticles of narrow size distribution are formed by spray-drying (**Fig. 1**). The particle size distribution is little affected by variations in the composition - in particular chitin and Ti contents - and the average diameter is about constant (average size of 2.5 µm). In contrast, the morphology of the particles changes importantly. SEM observations show that particles synthesized with low chitin volume fractions (i.e. ϕ_{CHI} = 0.15) have very smooth surfaces (**Fig. 1A)**. Surface roughness increases with increasing chitin volume fraction (**Fig. 1B and C)**, in agreement with former results on chitin-silica nano-composites.[10] Moreover, for materials prepared with a high chitin content (ϕ_{CHI} = 0.65), the spherical shape is lost and particles with a more complex morphology are formed with high surface roughness.

Texture

The evolution of nitrogen sorption behavior of calcined SiO_2/TiO_2-A materials as a function of chitin volume fractions is presented in **Fig. 2**. All samples present hysteresis loops related to the presence of mesopores. The shape of the loops is of type H2,[49] similar to those already obtained for pure mesoporous silica templated by the same sort α-chitin nanorods.[38] The main textural parameters (mesoporous volume, specific surface area and pore size) are found to rise with increasing chitin volume fraction, ϕ_{CHI} (**Table 1**). The pore volume fraction (ϕ_{POR}) is deduced from the maximum of sorption in nitrogen isotherms and is calculated using **Eq. 2**. From the nitrogen isotherms one can thus be deduce that in a range of ϕ_{POR} = 0.10-0.53, the BET surface area (S_{BET}) increases gradually from 70 to 445 $m^2\ g^{-1}$, whilst the average pore

size increases slightly from 5 to 6 nm (**Table 1**). For lowest ϕ_{POR} (= 0.10) tensile strength effect[50] is observed at p/p_0 = 0.45, which indicates that pores have formed as internal cavities and will thus not be accessible for larger molecules in this case (as was deduced from catalytic tests, see below).

Interestingly, the sorption isotherm of the sample with ϕ_{CHI} = 0.65 shows a profile different from the other samples. For this sample, in addition to the first hysteresis loop with an inflexion point on the desorption branch located near p/p_0 = 0.6 (V_{POR} = 0.60 mL.g^{-1}) a second hysteresis appears at higher partial pressure. This can be explained by chitin nanorods being in excess in the mixture with respect to siloxane oligomers, which therefore cannot fully cover the surface of the chitin nanorods. It should be noted that the critical ϕ_{CHI}* value above which α-chitin nanorods are not fully covered by silica has been estimated to be in the range 0.2-0.4.[42] Hence, some of the chitin nanorods can cling together during synthesis resulting in larger pores upon chitin removal (**Fig. 4J**). Similar features were also observed for porous silica without titanium, templated with α-chitin nanorods.[37,38]

To explore more in details the porosity of materials obtained with ϕ_{CHI} = 0.65, a mercury porosimetry analysis was carried out (**Fig. 3**). The interparticular filling is firstly observed up to a volume of 1.3 mL.g^{-1} (corresponding to a size of 100 nm - 5 µm). A sharp step is then followed which reveals a narrow size distribution of macropores within the particles (2.5 - 0.2 µm) corresponding to a macroporous volume of 1.3 mL.g^{-1} (2.6 - 1.3 = 1.3 mL.g^{-1}). This step is then followed by a plateau where the intrusion volume stays constant. A second, weaker step corresponds to the mercury intrusion into the mesoporosity within the sample showing a volume of 0.6 mL g^{-1} (3.2 - 2.6 = 0.6 mL.g^{-1}) thus confirming the results obtained by nitrogen sorption. In order to assess the mechanical stability of the sample the intrusion/extrusion cycle was repeated at high pressures. The shape of the second intrusion/extrusion cycle is very similar to the first one, suggesting that the particles are stable to a pressure as high as 4000 bars. This is not the case for other kind of mesoporous silica particles.[51]

Porosity has further been investigated by TEM (**Fig. 4**). The electron-clear structures reveal the presence of elongated pores within the oxide network, whose proportion increases with ϕ_{CHI}. Pore sizes estimated from TEM images are consistent with the dimensions of the pores calculated by the BdB method from the desorption branch in nitrogen sorption isotherms. Larger electron-clear features in the images (cracks) are microtomy artifacts and should thus be disregarded. We have observed that up to 10 mol% of Ti added (Si/Ti $\geq$ 9), complex textural parameters are not subjected to major variations and are similar to those obtained for pure siliceous materials.

Local structure

Fig. 5 shows a comparison of Ti 2p-photoelectron and UV-vis spectra of calcined SiO_2/TiO_2-A material (ϕ_{CHI} = 0.65, Si/Ti = 19) with those of TS-1 and anatase. The dominant XPS features are associated with the Ti $2p_{3/2}$ and Ti $2p_{1/2}$ peaks with a spin-orbital splitting between them of 5.7 eV characteristic for the Ti^{4+} valence state. However, Ti can be in different coordination states in the studied samples. For example, in the anatase crystal, the titanium atoms are in octahedral oxygen coordination (Ti_{Oh}) with Ti $2p_{3/2}$ binding energy at 458.6 eV (**Fig. 5C**). Also, it is known that in the structure of titanium silicalite TS-1 catalyst, the Ti atoms are in a tetrahedral coordination state (Ti_{Td}) and for this configuration we have measured a Ti $2p_{3/2}$ binding-energy of 460.5 eV (**Fig. 5B**). This large difference in the Ti $2p_{3/2}$ binding energies for the two coordination states allows to reliably determine the local Ti environment in the synthesized materials. In TS-1 that we use as standard for tetrahedral coordination, spectrum deconvolution suggests the existence of additional 2p-peaks at 458.2 and 463.9 eV (**Fig. 5B**), thus indicating the presence of small amounts of Ti_{Oh} atoms (about 8% of total Ti).

Similarly, the calcined samples exhibit a majority of Ti_{Td} sites, as visible in **Fig. 5A** where intense Ti $2p_{3/2}$- and Ti $2p_{1/2}$- peaks have been measured at 460.5 and 466.2 eV, respectively. A small amount of octa-coordinated Ti is also detected associated with weaker peaks at 458.3 and 464.0 eV, yielding a molar ratio Ti_{Td}/Ti_{Oh} of about 9.

Results obtained by DR UV-vis spectroscopy confirm the results of XPS modeling. The DR UV-vis spectrum of the SiO_2/TiO_2-A sample exhibits a main absorption band centered at 210 nm and a shoulder at 260 nm (**Fig. 5D**). The adsorption band at 210 nm is attributed to tetrahedral sites within the sample, since a strong absorption band is obtained at the same wavelength for TS-1 (**Fig. 5E**). On the contrary, the anatase sample shows a characteristic absorption band split into two maxima near 245 and 315 nm with a well defined absorption edge at 390 nm. These features, in agreement with typical anatase spectra are related to the O_2-Ti^{4+} charge transfer, and are not present in the spectra of our silica-titania materials.

SiO_2/TiO_2-A calcined samples made with different ϕ_{CHI} and/or Si/Ti ratios have also been studied by XPS. Systematically, the Si/Ti molar ratio estimated by XPS is well above the Si/Ti molar ratio of the bulk (**Table 2**). As XPS is mainly probing the samples surface at the nanometer scale, this can be understood as a preferential location of Ti atoms far from the microparticles surface, probably close to the pores generated by the chitin nanorods removal. Indeed, during the synthesis, the $Ti(O^iPr)_2(acac)_2$ precursor can interact with the chitin

nanorods surface, notably through the pending -OH or -NH_2 groups that can complex Ti^{4+} cations as deducted from chitosan-titania hybrid materials.[52] It can thus be interesting to exploit these possible Ti-chitin interactions in order to achieve SiO_2/TiO_2 catalysts with Ti active sites preferentially located at the pore surface.

2.2 Alternative syntheses of silica-titania catalysts (series B and C)

Chitin nanorods are usually stabilized in aqueous acidic media to prepare stable suspensions that were shown to exhibit liquid crystal properties.[44] We recently demonstrated that chitin nanorods can be stably dispersed in ethanol at low or moderate concentrations (below 10 wt%).[53] Therefore, we explored alternative synthesis routes where both precursors are suspended in ethanol and directly mixed thus avoiding time-consuming preparation steps. In particular, the elimination of water by solvent exchange and evaporation steps to avoid uncontrolled condensation and precipitation is no longer necessary. The resulting stable suspensions can be stored and readily processed at any time to elaborate materials, by spray-drying for instance. The materials obtained with chitin ethanolic suspensions are labeled as SiO_2/TiO_2-B and -C, depending on the order of precursors addition, as summarized in **Scheme 1**.

Texture

Nitrogen sorption isotherms for all synthesis procedures (series A, -B and -C) have been recorded for calcined materials (**Fig. 6**, **Table 3**). Comparing the nitrogen isotherms at different ϕ_{CHI} values reveals three important conclusions: a) the isotherms obtained for series B and C materials are very similar for equal ϕ_{CHI}, b) the isotherms of SiO_2/TiO_2-B and -C materials show higher nitrogen sorption volumes in the entire p/p_0 range compared to SiO_2/TiO_2-A materials at equal ϕ_{CHI} and c) the profile of the nitrogen isotherms is similar for all materials at constant ϕ_{CHI}.

Textural properties for materials synthetized with ϕ_{CHI} = 0.15, 0.33 and 0.65 are listed in **Table 3**. For materials synthesized with ϕ_{CHI} = 0.15 and 0.33, isotherms with defined porosities are obtained. In the case of ϕ_{CHI} = 0.15, the desorption relative pressure corresponds to the phenomenon of tensile strength effect at 0.45 p/p_0, thus the majority of formed pores should be inaccessible to larger molecules. For ϕ_{CHI} = 0.33 (**Fig. 6B**) capillary condensation is observed (with pore sizes of 5 nm for all materials). S_{BET} and pore volume increase considerably using ethanolic chitin suspension during the synthesis (**Table 3**). For higher ϕ_{CHI} values (i.e. 0.65, **Fig. 6C**) hierarchical porous systems are obtained with a primary porosity

resulting from the imprint of isolated chitin monocrystals (pore size ~5 nm) and a second porosity with mesopore sizes above 15 nm (see mercury porosimetry, **Fig. 3**). Profiles of the nitrogen isotherms for both processes at ϕ_{CHI} = 0.65 are very similar, but here again higher specific surface areas are achieved for the SiO_2/TiO_2-B and -C samples, as high as 590 $m^2.g^{-1}$. As deduced from nitrogen sorption (**Table 3**), the synthesis procedures using chitin suspensions in ethanolic medium (series B and C) invariably result in higher specific surface areas and pore volumes compared to samples obtained with the aqueous chitin suspensions (series A). This might be related to the presence of water in the early steps of the synthesis route A, before its azeotropic removal, which may affect the chemical stability of siloxane oligomers and partially interfere with colloidal interactions between chitin nanorods and siloxane oligomers. Although the proportion of Ti is low, we might also consider the effect of the different procedures on the interactions of chitin and siloxane oligomers with $Ti(O^iPr)_2(acac)_2$. Furthermore the relation between ϕ_{CHI} and ϕ_{POR} has been studied for the obtained materials (**Fig. 7**). For the SiO_2/TiO_2-A materials, pore volume fraction (ϕ_{POR}) linearly correlates to chitin volume fraction (ϕ_{CHI}) with $\phi_{POR} = 0.79\phi_{CHI}$. For series SiO_2/TiO_2-B and -C, the proportionality factor is very close to one, $\phi_{POR} \approx \phi_{CHI}$, indicating that nearly all the chitin introduced in the initial mixture participates to the creation of porosity. This again points out the possible role of small amounts of water initially present in route A in creating inhomogeneities, while the same process in the absence of water (series -B and -C) yields very homogeneous hybrid samples.

Local structure

For SiO_2/TiO_2-B and SiO_2/TiO_2-C materials there is a significant difference in color of the prepared solutions prior to spray-drying. Precursor solutions to obtain SiO_2/TiO_2-C show a less intense coloration than SiO_2/TiO_2-B precursor solutions (yellow colour comes from the complexation of Ti with acetylacetonate (acac)). This gives an indication that more Ti^{4+} cations have possibly been complexed by chitin surface groups in the series C solution compared to the series B (and after spray-drying and calcination more Ti sites could be closer to the pore surface). Unfortunately we were not able to quantify the amount of free Ti-complex in solution by UV-visible spectroscopy, as the α-chitin nanorods themselves diffuse over a wide spectrum, overlapping with adsorption from the Ti-complex.

XPS was used to gain insight into the distribution and environment of Ti sites, in relation with the synthesis procedure and interactions between the precursors. We have estimated surface Si/N molar ratios by XPS and compared them to bulk Si/N molar ratios for non calcined B

and C samples (**Table 4**). Surface Si/N ratios are always higher than bulk ones, which reflects the internal organisation of the samples where chitin nanorods (N containing domains) are covered by a siloxane network. We also notice that for the C series, Si/N ratios are higher than for the B series, indicating a stronger phase separation between chitin nanorods and the siloxane network. We have also checked the Si/Ti molar ratios on non calcined and calcined samples (**Table 4**). Interestingly, we observe that surface Si/Ti ratios are always higher than bulk ratios for series C samples as shown earlier for sample A (**Table 2**), but different to sample B (it only occurs at low Si/Ti in this case). For series C, there is thus again a preferential location of Ti away from the microparticles surface, probably close to the pores made by the chitin nanorods. These differences between series A, B and C in porosity and Ti location will greatly influence the accessibility of the active sites, and therefore the catalytic performances of the materials.

2.3 Catalysed sulfoxidation reactions

The catalytic behaviour of the synthesized silica-titania materials was evaluated in the mild oxidation of methyl-phenyl sulfide (MPS) and dibenzothiophene (DBT) with hydrogen peroxide. The main oxidation products (representing more than 95% of product mixture) are displayed in **Scheme 2** for each reaction. The oxidation of sulfides and thiophene derivatives can be considered as model reactions for two important industrial applications: sulfoxides/sulfones synthesis and sulfur removal from fuels.[4,54,55] The typical kinetic profiles for the oxidation of MPS and DBT are plotted in **Fig. 8a** and **8b**, respectively. The oxidation of MPS led to the sulfoxide and sulfone as products. On the contrary, the kinetic profile of the DBT oxidation showed that the sulfone was selectively formed; only traces of sulfoxide were found among the oxidation products at low levels of DBT conversion. Taking into account the previous results obtained on various catalysts,[4,56,57] it is reasonable to assume that the product of the first stage in the oxidation with H_2O_2 is the DBT sulfoxide, but it is rapidly converted into sulfone in a second oxidation step.

To obtain information about the effect of the catalyst porosity, the oxidation of MPS and DBT was carried out over SiO_2/TiO_2-A catalysts with variable ϕ_{POR} and constant molar ratio of Si/Ti = 19. The experimental data are summarized in **Table 5**. As previously reported,[1] for both molecules a strong and almost linear dependence between the conversion and the ϕ_{POR} was observed. Thus, after 50 min of reaction time, the conversion of MPS into sulfone was 13% and 98% for ϕ_{POR} = 0.10 and 0.53, respectively.

As far as initial reaction rates are concerned, they follow an exponential increase from 0.02 to 0.25 mmol.min^{-1}.g^{-1} for ϕ_{POR} = 0.10 and 0.53, respectively. For comparison the oxidation of DBT in the presence of the TS-1 zeolite gave very low conversion (2% after 120 min) with a corresponding productivity of 0.007 mmol.min^{-1}.g^{-1}.

As known, the efficiency in catalysis is proportional to the accessibility to active sites when the system is outside of diffusion limitations. An increase in catalytic efficiency can thus be obtained by increasing the amount of accessible active sites. This can be achieved either by increasing the number of active sites on the surface or by increasing the specific surface area and thus increasing the total amount of active sites.

As discussed above, by changing the synthesis conditions (all ethanol), SiO_2/TiO_2-B and SiO_2/TiO_2-C, mixed oxides with improved characteristics were obtained. These materials should be catalytically more active than the SiO_2/TiO_2-A materials, as they show higher specific surface areas and should thus have more accessible Ti sites. **Fig. 9** compares the performances in the MPS oxidation of the catalysts A, B and C with Si/Ti = 19

and ϕ_{CHI} = 0.15, 0.33 and 0.65. The initial reaction rates are plotted in **Fig. 9A**, the productivities (in mmol of MPS converted per min and g of catalyst) after 30 min are plotted in **Fig. 9B** and the initial reaction rates normalized by specific surface area are showed in **Fig. 9C**.

As expected, the initial reaction rate and the productivity increase as ϕ_{CHI} is increased from 0.15 to 0.65, mostly reflecting the increase in surface area. Also, there is no significant distinction between the different samples at ϕ_{CHI} = 0.15. This can be explained by the lack of accessibility of most of the internal surface. In contrast, at ϕ_{CHI} = 0.33 and 0.65 the initial reaction rate for the SiO_2/TiO_2-C catalyst is significantly higher compared to SiO_2/TiO_2-B and -A. The same tendency is observed in termes of productivity at ϕ_{CHI} = 0.33. Productivities at high initial chitin volume fraction (i.e. ϕ_{CHI} = 0.65) are similar for SiO_2/TiO_2-B and -C, and higher than for SiO_2/TiO_2-A.

Except at low ϕ_{CHI} = 0.15, the initial reaction rate normalized by the specific surface area is highest for SiO_2/TiO_2-C materials (**Fig. 9C**). Therefore, initial mixing of the Ti precursor with chitin nanorods (series C) makes the resulting materials more efficient than the two others types (series A and B) by a factor of 1.4 and 1.2 for ϕ_{CHI} = 0.33 and 0.65, respectively. This should be related to the enrichment in Ti sites near the pore surface, as suggested by XPS measurements (**Table 4**), possibly resulting from complexation of Ti atoms by chitin surface groups. For the samples of series A and B at these two compositions, very similar values of V_{int}/S_{BET} are obtained, underlying the direct role of higher surface area in the increase of the

initial rate (**Fig. 9A**). Surprisingly, in the particular case of ϕ_{CHI} = 0.15, the highest value of V_{int}/S_{BET} is obtained for SiO_2/TiO_2-A. We attribute this apparently higher efficiency to the much higher surface area measured for samples -B and -C taken into account by the normalization, a large proportion of which being non-accessible internal porosity.

Effect of the Ti content

In order to emphasize the effect of the Ti amount in catalysts, between the initial reaction rate and the specific surface area, are summarized in **Table 6**.

The comparison in terms of initial reaction rate reveals that SiO_2/TiO_2-C samples always have higher values than the other catalysts. It is important to note that for SiO_2/TiO_2-C with Si/Ti = 68 the same initial rate is obtained as for SiO_2/TiO_2-A with Si/Ti = 38. In other words, with the new synthesis procedure (SiO_2/TiO_2-C materials), the total amount of Ti introduced can be cut in half while maintaining the same initial reaction rate. Concerning the productivity at 30 min of reaction, it is 0.86 $mmol.min^{-1}.g^{-1}$ for SiO_2/TiO_2-A, and about 1 $mmol.min^{-1}.g^{-1}$ for SiO_2/TiO_2-B and -C. A similar order of activity is observed for samples with Si/Ti = 38 but with overall slightly lower productivities. For the system with the lowest amount of Ti (i.e. Si/Ti = 68) the value of P30 for SiO_2/TiO_2-B and -C is twice that exhibited by the SiO_2/TiO_2-A sample.

Again, normalization of initial reaction rates by specific surface area shows that the increase in productivity, V_{int} is due to the increase of the specific surface area for SiO_2/TiO_2-B compared to SiO_2/TiO_2-A. Hence, in this case, increase in active site accessibility is directly related to the increase in surface area. The situation is different for SiO_2/TiO_2-C samples, where higher V_{int}/S_{BET} values are obtained for all Si/Ti ratios. This reinforces the conclusion that syntheses performed in ethanol (-B and -C) yield more porosity than when water is initially present in the system. In addition, the mixing and interaction of Ti precursors with chitin particles prior to adding the siloxane oligomers (route -C) favors the distribution of Ti sites near the pore surface by a factor of 1.2, 1.3 and 1.4 for Si/Ti ratios of 19, 38 and 68 respectively, compared to routes -A and -B.

Recycling of catalysts

Catalyst recycling experiments were performed in order to evaluate the stability of catalysts during exploitation. SiO_2/TiO_2-A, -B and -C synthesized with ϕ_{CHI} = 0.33 and Si/Ti = 19 were reused five times in the MPS oxidation reaction at 333 K, in acetonitrile, for 50 min. The catalyst was separated by filtration after each reaction, washed with acetonitrile, and then

placed into a fresh reagent mixture. As can be deduced from **Fig. 10A** the productivities after 50 minutes of reaction stays high for the first five runs showing only slight deactivation. Deactivation affects all samples in a similar manner, suggesting that the deactivation mechanism is probably similar. After five catalytic cycles, SiO_2/TiO_2-C exhibited comparable productivity as the SiO_2/TiO_2-A sample during the first run (i.e 0.36 $mmol.min^{-1}.g^{-1}$). Diffuse reflectance UV-vis spectra recorded before and after the catalytic tests for the SiO_2/TiO_2-A material (**Fig. 10B**) showed a slight shift towards higher wavelengths of the low energy band, which indicates a change in the Ti coordination environment. In agreement with that, we noticed a drop in the Ti_{Td}/Ti_{Oh} ratio estimated from XPS from about 11 to 4 after the catalytic tests (the XPS Si/Ti molar ratio remaining in the 32-34 range).

Comparison with the literature

The catalytic performance of these materials was further compared to those previously reported for the oxidation of MPS under same conditions. A Ti-MCM-41 catalyst (S_{BET} = 795 $m^2.g^{-1}$, Si/Ti = 112) gave a conversion of 36% after 60 min of reaction which corresponds to a productivity of 0.18 $mmol.min^{-1}.g^{-1}$ at that reaction time.[54] A SiO_2-TiO_2 obtained via non-hydrolytic sol-gel techniques (S_{BET} = 1215 $m^2.g^{-1}$, Si/Ti = 22) yielded full conversion after 45 min and has a productivity of 0.67 mmol min^{-1} g^{-1} at full conversion for the MPS oxidation.[43] For our materials, the highest productivity at full conversion (attained after only 30 min) reaches 1 mmol min^{-1} g^{-1} for the sample at ϕ_{POR} = 0.49 (S_{BET} = 590 $m^2.g^{-1}$, Si/Ti = 19), which is three times higher than for the above mentioned catalysts when normalized by surface area. This finding underlines the efficiency of these materials for mild sulfoxidation which should be ascribed to enhanced diffusivity in the system of interconnected mesopores and to a very good distribution of the Ti sites within the material.

3. Experimental

3.1 Syntheses

Materials

Chitin flakes extracted from shrimp shells were kindly provided by France Chitin.[58] TEOS (ABCR, purity > 99.9%), absolute ethanol (Sigma-Aldrich, purity > 99.8%), $Ti(OiPr)_2(acac)_2$ (Sigma-Aldrich, 75wt% in isopropanol), anatase (Sigma-Aldrich, > 99%), methyl-phenyl sulfide (Sigma-Aldrich, purity > 99%), dibenzothiophene (Sigma-Aldrich, purity > 98%), hydrogen peroxide (Sigma-Aldrich, 50 wt% aqueous solution), and acetoniltrile (Fisher

Chemical, HPLC Gradient grade, 15 mL) were used as received. TS-1 was synthesized according to the literature.[59]

Chitin suspensions

Aqueous suspensions of *α*-chitin nanorods were prepared following a procedure described elsewhere (ref. 44, Belamie *et al*. 2004), based on the hydrolysis of chitin in boiling HCl (4 M) for 120 min. The nanorods preparation involves elimination of excess HCl by dialysis, followed by ultrasound dispersion prior to the purification by low- and high-speed centrifugation cycles. Nanorods are finally suspended in HCl (10^{-4} M) or EtOH at a concentration of 1.5 wt%.

Siloxane oligomers sols

An alcoholic solution containing siloxane oligomers (3 mmol.g^{-1}) was obtained by mixing under reflux (4 h) TEOS and water in absolute ethanol with the molar composition 1 TEOS: 2 H_2O: 2 EtOH. The resulting siloxane oligomers are small colloids with an average hydrodynamic diameter of D_h = 2.9 ± 0.2 nm determined by DLS.

Silica-titania materials

For the preparation of the silica-titania hybrid materials the siloxane solution was mixed with $Ti(OiPr)_2(acac)_2$ and the chitin suspension. The reactant proportions are set to reach the water-ethanol azeotrope composition (ca. 96wt% ethanol) and a given chitin volume fraction ϕ_{CHI} in the final nano-composites.

SiO_2/TiO_2-A: For a typical procedure, in order to obtain a material with ϕ_{CHI} = 0.65 and 5 mol% Ti, the siloxane suspension (3 g, n_{Si} = 8.88 mmol) was placed in a round bottom flask (1 *l*) and stirred. $Ti(OiPr)_2(acac)_2$ (0.228 g, n_{Ti} = 0.469 mmol) was added dropwise at RT. The yellow mixture was stirred for additional 5 min and the chitin suspension (22.5 ml) was added dropwise forming a yellow/orange precipitate. The precipitate was dissolved by adding immediately 400 mL of absolute ethanol and stirring. The solvent mixture is evaporated using standard rotary evaporation conditions until the solution transforms into a paste. The same initial amount of ethanol is then added and the mixture is again evaporated. These solvent-exchange cycles are repeated three times to ensure complete removal of water. After the last ethanol removal, the resulting paste was dissolved in ethanol in order to achieve a chitin concentration of 3.10^{-3} g.mL^{1}.

SiO_2/TiO_2-B: Amounts of precursor materials were the same as above. The siloxane suspension was mixed to $Ti(OiPr)_2(acac)_2$ under stirring, and followed by the addition of a

chitin suspension in ethanol. Evaporation cycles for solvent exchange were not necessary in this case.

SiO_2/TiO_2-C: Amounts of precursor materials were the same as above. A chitin suspension in EtOH was first mixed with $Ti(OiPr)_2(acac)_2$ during 10 min under stirring, followed by the addition of the siloxane suspension. Evaporation cycles for solvent exchange were not necessary in this case.

The obtained solutions were subsequently spray-dried using a Büchi 290 mini-spray dryer under dry nitrogen at 393 K. Mesoporous samples were obtained by calcination in air (8 h, 823 K). After calcination, the siloxane condensation degree may slightly increase (from about 0.88 to 0.91 as determined by ^{29}Si solid-state NMR on some samples). The molar ratio Si/Ti determined by elemental analyses on different calcined and non calcined samples coincide with the initial ratio inside the sols as expected.

3.2 Characterization techniques

Elemental analyses were done at the CNRS facility "Service Central d'Analyse" (Vernaison, France).

Nitrogen sorption isotherms were recorded using a Micrometrics Tristar apparatus at 77 K. Calcined samples were outgased at 523 K at $3 \cdot 10^{-3}$ Torr for at least 8 h. The pore volume fractions ϕ_{POR} were estimated using the maximum adsorbed volume of nitrogen sorption isotherms considering a density of 2.2 g cm^{-1} for silica. Specific surface areas (S_{BET}) were calculated using the BET method.[60] Average pore diameters were inferred from the nitrogen desorption branch according to Broekhoff and de Boer (BdB).[61]

Transmission Electron Microscopy (TEM) analyses were made on a JEOL 1200 EX2 microscope operating at 100 kV. Calcined samples were grounded and embedded in a resin and cut into slices (~70 nm thick) with an ultramicrotome.

Scanning Electron Microscopy (SEM) images were recorded using a Hitachi S-4500 I SEM.

Diffuse reflectance UV-vis (DR UV-vis) spectra were recorded under ambient conditions on a Perkin Elmer Lambda 14 spectrometer equipped with a $BaSO_4$ coated integration sphere. Samples were diluted in $BaSO_4$; spectra were plotted using Kubelka-Munk function.

X-ray photoelectron spectroscopy (XPS) measurements were carried out on an ESCALAB Mk II (VG Scientific Ltd) electron spectrometer (base vacuum of 10^{-8} Pa). XPS spectra were recorded using a Mg K_α excitation source with photon energy of 1253.6 eV. The instrumental resolution was 1.06 eV (from the FWHM of Ag3d5/2 photoelectron line). Energy calibration was performed using the C 1s line of adsorbed hydrocarbons (285 eV). The relative

concentrations of the different chemical species were determined by normalization of the areas of the XPS peaks by their photoionization cross-sections calculated by Scofield.[62]
Microparticles grain size was measured by light scattering on a MALVERN Mastersizer 2000 in water dispersions.

3.3 Catalytic studies

The catalytic experiments were carried out at atmospheric pressure, at 333 K, in a three-necks glass batch reactor (50 ml), equipped with magnetic stirrer, thermometer and condenser, and placed in a thermostated bath. The solid catalyst was suspended under vigorous stirring (1000 rpm) in a mixture containing the organic substrate (1.5 mmol), hydrogen peroxide (50 wt% aqueous solution, 3 mmol for MPS and 7.5 mmol for DBT) and acetoniltrile (15 mL) as solvent. Blank experiments were carried out in the absence of catalyst. Samples of the reaction mixture were withdrawn periodically and analyzed on a Varian 3900 chromatograph equipped with a capillary column (DB-1, 60 m, 0.20 mm i.d., 0.25 µm film thickness) and FID.

3.4 Methods

Estimation of chitin volume fraction (ϕ_{CHI}) *and pore volume fraction* (ϕ_{POR})

The composition of the initial suspensions used to prepare the materials was set to reach a given chitin volume fraction (ϕ_{CHI}) in the final nano-composites. ϕ_{CHI} is calculated using the volumes (V) of the components, and is described as:

$$\phi_{CHI} = \frac{V_{Chitine}}{V_{Chitin} + V_{SiO_2} + V_{TiO_2}} \quad (1)$$

The volume occupied by each component in the final material after drying is obtained by dividing the mass of this component by its estimated density within the solid (i.e. ρ_{Chitin} = 1.43, ρ_{SiO2} = 1.9, ρ_{TiO2}= 4).

The pore volume fraction (ϕ_{POR}) is deduced from the plateau of sorption after capillary condensation in nitrogen sorption isotherms and is calculated as:

$$\phi_{POR} = \frac{V_{POR}}{V_{Sample} + V_{POR}} \quad (2)$$

with V_{POR}: maximal volume in nitrogen isotherms and V_{Sample}: mass sample/density sample (for the materials herein described, a density of 1.9 was used.

Initial velocity and productivity

By applying a tangent to the initial part of the conversion vs. time curve, where conversion is linear in time, the initial velocity can be calculated as the slope (*a*) of the linear relation and is given as:

$$C = a \cdot t \tag{3}$$

with *C*: conversion in %, *t*: time in min.

From this relation the initial velocity (υ_{int}) is calculated by:

$$\upsilon_{int} = a\frac{n}{m} \cdot 0.01 \tag{4}$$

with *n*: moles of reactant and *m*: mass of catalyst.

Productivity (P_t) is calculated for a certain time (*t*) of the reaction as:

$$P_t = \frac{C \cdot n}{t \cdot m} \cdot 0.01 \tag{5}$$

with *C*: conversion (%), *n*: moles of reactant, *t*: time of reaction, *m*: mass of catalyst.

4. Conclusion

In summary, we have obtained mesoporous silica-titania catalysts synthesized by combining the sol-gel process with the self-assembly properties of α-chitin nanorods, acting as green templates. Spray-drying allowed for the achievement of catalysts as individual microparticles. The three synthesis methods presented here let to the conclusion that materials synthesized employing an initial ethanolic chitin suspension present the advantage of an easy and fast synthesis protocol leading to materials with increased textural properties and higher catalytic activity. Moreover, by mixing the α-chitin nanorods first with the titanium complex prior to combination with the siloxane oligomers, the quantity of active titania sites on the surface can be maximized, leading to materials with very high productivities in sulfoxidation reactions. This important result can be explained by the complexing ability of the chitin surface towards the titanium monomeric precursor. Hence, we are currently investigating the interactions of metal complexes and chitin nanorods in order to conceive other materials with optimized properties. We are certain that the chitin bio-templating strategy described here represents a valuable tool for directing active sites on the surface of mixed oxides, in addition to the modulation of the textural properties coming from the hard templating approach.

Acknowledgements

ANR French Agency is acknowledged for the specific funding through the HYSIKIT project. Campus France is acknowledged for its support through the PHC program Rila. Thomas Cacciaguerra is thanked for his help on electron microscopies.

Bibliographic references and notes

1. A. Sachse, V. Hulea, K. L. Kostov, N. Marcotte, M. Yu Boltoeva, E. Belamie and B. Alonso, *Chem. Commun*., 2012, **48**, 10648-10650.
2. K. Kaczorowska, Z. Kolarska, K. Mitka and P. Kowalski, *Tetrahedron*, 2005, **61**, 8315-8327.
3. E. Ito and J. A. R. Van Veen, *Catal. Taday*, 2006, **116**, 446-460.
4. V. Hulea, F. Fajula and J. Bousquet, *J. Catal.*, 2001, **198**, 179-186.
5. H. Lü, J. Gao, Z. Jiang, Y. Yang, B. Song and C. Li, *Chem. Commun.*, 2007, 150-152.
6. I. Fernandez and N. Khiar, *Chem. Rev.*, 2003, **103**, 3651-3705.
7. D. R. C. Huybrechts, L. De Bruycher and P. A. Jacobs, *Nature*, 1990, **345**, 240-242.
8. G. Bellussi, A. Carati, M. G. Clerici, G. Meddinelli and R. Millini, *J. Catal*., 1992, **133**, 220-230.
9. S. Gontier and A. Tuel, *Appl. Catal. Gen.*, 1994, **118**, 173-186.
10. M. G Clerici and M. E. Domine, in *Liquid Phase Oxidation via Heterogeneous Catalysis: Organic Synthesis and Industrial Applications*, eds. M. C. Clerici and O. A. Kholdeeva, Wiley, Weinheim, 2013, pp. 21-93.
11. O. A. Kholdeeva, in *Liquid Phase Oxidation via Heterogeneous Catalysis: Organic Synthesis and Industrial Applications,* eds. M. C. Clerici and O. A. Kholdeeva, Wiley, Weinheim, 2013, pp. 127-220.
12. T. Blasco, A. Corma, M. T. Navarro and J. Pérez Pariente, *J. Catal.*, 1995, **156**, 65-74.
13. A. Corma, M. Domine, J. A. Gaona, J. L. Jordá, M. T. Navarro, F. Rey, J. Pérez-Pariente, J. Tsuji, B. McCulloch and L. T. Nemeth, *Chem. Commun*., 1998, 2211-2212.
14. W. Zhang and T. P. Pinnavaia, *Catal. Lett*., 1996, **38**, 261-265.
15. C. Galacho, M. M. L. Ribero Carrott and P. J. M. Carrott, *Microporous Mesoporous Mater*., 2007, **100**, 312-321.
16. M. Guidotti, C. Pirovano, N. Ravasio, B. Lázaro, J. M. Fraile, J. A. Mayoral, B. Coq and A. Galarneau, *Green Chem*., 2009, **11**, 1421-1427.
17. N. Ravasio, F. Zaccheria, M. Guidotti and R. Psaro, *Top. Catal.*, 2004, **27**, 157-168.
18. R. Huttler, T. Mallat and A. Baiker, *J. Catal.*, 1995, **153**, 177-189.
19. R. J. Davis and Z. F. Liu, *Chem. Mater*.,1997, **9**, 2311-2324.
20. M. Andrianainarivelo, R. Corriu, D. Leclercq, P. H. Mutin and A. Vioux, *J. Mater. Chem.*, 1996, **6**, 1665-1671.
21. V. Lafond, P. H. Mutin and A. Vioux, *J.Chem. Mater*., 2004, **16**, 5380-5386.

22. J. H. Clark, *Green Chem.*, 1999, **1**, 1-8.
23. M. Eissen, J. O. Mertzger, E. Schmidt and U. Schneidewind, *Angew. Chem. Int. Ed.***,** 2002, **41**, 414-436.
24. N. Baccile, F. Babonneau, B. Thomas, T. Coradin, *J. Mater. Chem.*, 2009, **19**, 8537-8559.
25. J. M. Campelo, D. Luna, R. Luque, J. M. Marinas and A. A. Romero, *Chem. Sus. Chem*., 2009, **2**, 18-45.
26. R. Chal, C. Gerardin, M. Bulut and S. van Donk, *Chem. Cat. Chem*., 2011, **3**, 67-81.
27. C. Gerardin, J. Reboul, M. Bonne and B. Lebeau, *Chem. Soc. Rev*., 2013, **42**, 4217-4255.
28. S. Mann, *Nature*, 1993, **365**, 499-505.
29. H. Yang, N. Coombs and G. A. Ozin, *Nature*, 1997, **386**, 692-695.
30. S. Mann, in *Biomineralization. Principles and Concepts in Bioinorganic Materials Chemistry*, Oxford University Press, Oxford, 2001.
31. C. Sanchez, H. Arribart and M. M. G. Guille, *Nat. Mater*., 2005, **4**, 277-288.
32. E. Ruiz-Hitzky, M. Darder, P. Aranda and K. Ariga, *Adv. Mater*., 2010, **22**, 323-336.
33. H. Ehrlich, *Int. Geo. Rev*., 2010, **52**, 661-699.
34. N. Lin, J. Huang and A. Dufresne, *Nanoscale*, 2012, **4**, 3274-3294.
35. A. El Kadib, M. Bousmina and D. Brunel, *J. Nanoscience Nanotechnology*, 2014, **14**, 308-331.
36. E. Dujardin, M. Blaseby and S. Mann, *J. Mater. Chem*., 2003, **13**, 696-699.
37. B. Alonso and E. Belamie, *Angew. Chem. Int. Ed.*, 2010, **49**, 8201-8204.
38. E. Belamie, M. Y. Boltoeva, K. Yang, T. Cacciaguerra and B. Alonso, *J. Mater. Chem.*, 2011, **21**, 16997-17006.
39. C. Schütz, J. Sort, Z. Bacsik, V. Oliynyk, E. Pellicer, A. Fall, L. Wågberg, L. Berglund, L. Bergström and G. Salazar-Alvarez, *PLOS ONE*, 2012, **7**, e45828.
40. N. Thanh-Dinh, K. E. Shopsowitz and J. M. MacLachlan, *Chemistry Eur. J.*, 2013, **19**, 15148-15154.
41. N. Thanh-Dinh, K. E. Shopsowitz and J. M. MacLachlan, *J. Mater. Chem. A*, 2014, **2**, 5915-5921.
42. A. Ivanova, D. Fattakhova-Rohlfing, B. E. Kayaalp, J. Rathouský and T. Bein, *J. Am. Chem. Soc*., 2014, **136**, 5930-5937.
43. J. F. Revol and R. H. Marchessault, *Int. J. Biol. Macromol.* **1993**, *15*, 329-335.

44. E. Belamie, P. Davidson and M. M. Giraud-Guille, *J. Phys. Bhem. B*, 2004, **108**, 14991-15000.
45. K. Masters, in *Spray-Drying in Pracice*, SprayDryConsult International ApS, Hvidovre, 2002.
46. C. Boissiere , D. Grosso , A. Chaumonnot , L. Nicole and C. Sanchez, *Adv. Mater*., 2011, **23**, 599-623.
47. B. Alonso, E. Véron, D. Durand, D. Massiot and C. Clinard, *Microporous Mesoporous Mater*., 2007, **106**, 76-94.
48. M. Fatnassi, C. Tourné-Pé teilh, T. Cacciaguerra, P. Dieudonne, J.-M. Devoisselle and B. Alonso, *New J. Chem*., 2010, **34**, 607-610.
49. K. S. W. Sing, *IUPAC Technical Reports and Recommendations*, 1985, **57**, 603-619.
50. J. C. Groen, L. A. A. Peffer and J. Perez-Ramirez, *Micropor. Mesopor. Mater*., 2003, **60**, 1-17.
51. J. Iapichella, J.-M. Meneses, I. Beurroies, R. Denoyel, Z. Bayram-Hahn, K. Unger and A. Galarneau, *Microporous Mesoporous Mater*, 2007, **102**, 111-121.
52. A. El Kadib, K.Molvinger, T. Cacciaguerra, M. Bousmina and D. Brunel, *Microporous Mesoporous Mater*., 2011, **142**, 301-307.
53. M. Boltoeva, I. Dozov, P. Davidson, K. Antonova, L. Cardoso, B. Alonso and E. Belamie, *Langmuir*, 2013, **29**, 8208-8212.
54. V. Hulea, P. Moreau and F. Di Renzo, *J. Mol. Catal*., 1996, **111**, 325-332.
55. V. Hulea, A. L. Maciuca, F. Fajula and E. Dumitriu, *Appl. Catal*. A, 2006, **313**, 200-207.
56. A. M. Cojocariu, P. H. Mutin, E. Dumitriu, F. Fajula, A. Vioux and V. Hulea, *Chem. Commun.*, 2008, 5357-5359.
57. Y. Jia, G. Li and G. Ning, *Fuel Process. Technol*., 2011, **92**, 106-111.
58. France Chitine, http://www.france-chitine.com (accessed July 2014).
59. *Verified Synthesis of Zeolitic Materials*, ed. H. Robson, Elsevier, Amsterdam, 2nd ed., 2001, p. 207.
60. S. Brunauer, P. H. Emmett and E. Teller, *J. Am. Chem. Soc.*, 1938, **60**, 309-319.
61. C. P. Broekhoff and J. H. De Boer, *J. Catal*., 1968, **10**, 377-390.
62. J. H. Scofield, *J. Electron Spectrosc. Relat. Phenom*., 1976, **8**, 129-137.

Tables

Table 1. Properties of SiO_2/TiO_2-A materials with Si/Ti = 19.

Initial ϕ_{CHI}	Final ϕ_{POR}	S_{BET} ($m^2.g^{-1}$)	V ($mL.g^{-1}$)	Average pore size (nm)
0.15	0.10	72	0.06	5.0
0.25	0.17	91	0.09	5.1
0.33	0.24	170	0.17	5.4
0.50	0.34	256	0.27	5.7
0.65	0.53	443	0.60	6.0

Table 2. Molar ratio Si/Ti for SiO_2/TiO_2-A calcined samples.

ϕ_{CHI}	bulk Si/Ti	surface Si/Ti (XPS)
0.15	19	~36
0.33	19	~33
0.65	19	~34
0.65	39	~70
0.65	70	~112

Table 3. Comparison of textural properties for SiO_2/TiO_2-A, -B and -C materials as function of initial chitin volume fraction ϕ_{CHI} (with Si/Ti = 19).

ϕ_{CHI}	ϕ_{POR}			S_{BET} ($m^2.g^{-1}$)			V ($mL.g^{-1}$)			Pore size (nm)		
	A	B	C	A	B	C	A	B	C	A	B	C
0.15	0.10	0.15	0.15	72	210	220	0.06	0.10	0.09	5	5	5
0.33	0.24	0.34	0.34	170	265	259	0.17	0.27	0.29	6	6	6
0.65	0.53	0.61	0.62	443	590	585	0.60	0.82	0.84	6; 30	6; 30	6; 30

Table 4. Si/Ti and Si/N molar ratio for SiO_2/TiO_2-B and -C non calcined and calcined samples (ϕ_{CHI} = 0.65).

Type of sample	bulk Si/Ti	surface Si/Ti (XPS)	bulk Si/N	surface Si/N (XPS)
B non calcined	19	~28	2.4	~4.4
B non calcined	39	~26	2.4	~5.1
B non calcined	70	~55	2.4	~4.9
C non calcined	19	~40	2.4	~19.5
C non calcined	39	~61	2.4	~12.4
C non calcined	70	~90	2.4	~8.9
B calcined	19	~130		
B calcined	39	~36		
B calcined	70	~62		
C calcined	19	~31		
C calcined	39	~52		
C calcined	70	~90		

Table 5. The effect of the catalyst porosity on the sulfoxidation of MPS and DBT; catalyst SiO_2/TiO_2-A (Si/Ti = 19).

	ϕ_{POR}				
	0.10	0.17	0.24	0.34	0.53
MPS conversion into sulfone [a] (%)	13	39	60	78	98
MPS initial rate ($mmol.min^{-1}.g^{-1}$)	0.41	0.95	1.57	2.09	4.32
DBT conversion [b] (%)	5	21	40	52	69
DBT initial rate ($mmol.min^{-1}.g^{-1}$)	0.02	0.04	0.06	0.14	0.25

a: reaction time = 50 min; b: reaction time = 120 min

Table 6. Catalytic behaviour of SiO_2/TiO_2 samples with ϕ_{CHI} = 0.65 and various texture and chemical composition for the MPS oxidation with H_2O_2.

	Si/Ti = 19			Si/Ti = 38			Si/Ti = 68		
	A	B	C	A	B	C	A	B	C
V_{int} ($mmol.min^{-1}.g^{-1}$)	1.29	1.69	1.98	1.19	1.45	1.87	0.56	0.84	1.16
P_{30} ($mmol.min^{-1}.g^{-1}$)	0.86	0.99	1.00	0.78	0.81	0.91	0.33	0.61	0.67
V_{int}/S_{BET} ($mmol.min^{-1}.m^{-2}$)	2.9	2.9	3.4	2.7	2.5	3.2	1.3	1.4	2.0

Schemes and Figures

Scheme 1. The three synthesis routes to elaborate SiO_2/TiO_2-A, -B and -C materials.

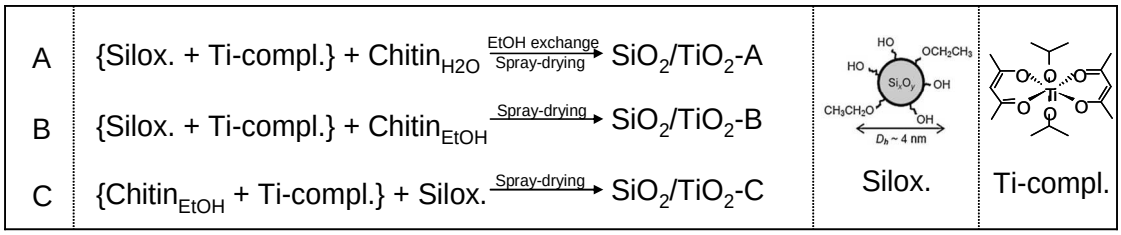

Scheme 2. Catalytic sulfoxidations of methyl-phenyl sulphide (MPS) and dibenzothiophene (DBT).

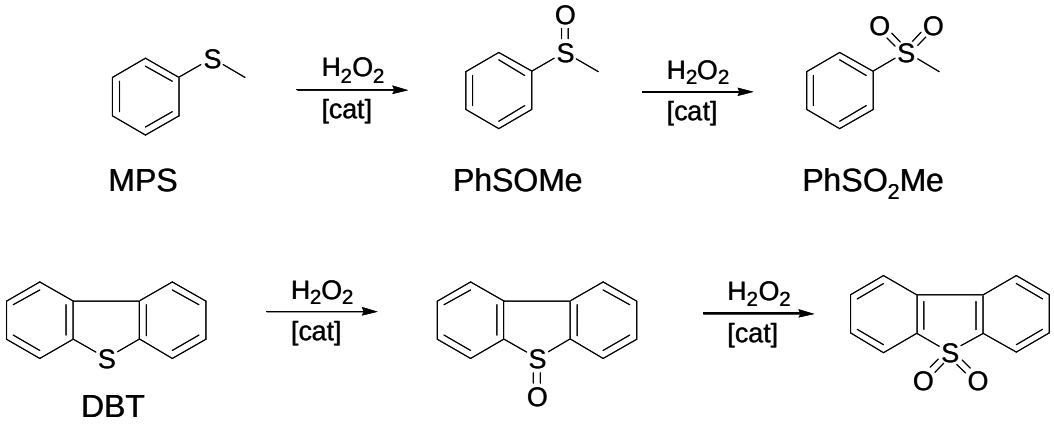

Fig. 1. SEM images of microparticles obtained by spray drying for ϕ_{CHI} = 0.15 (a), 0.33 (b) and 0.65 (c). Experimental size distribution of microparticles (d) (■: ϕ_{CHI} = 0.65 and Si/Ti = 19, ▲: ϕ_{CHI} = 0.65 and no Ti, □: ϕ_{CHI} = 0.25 and Si/Ti = 19).

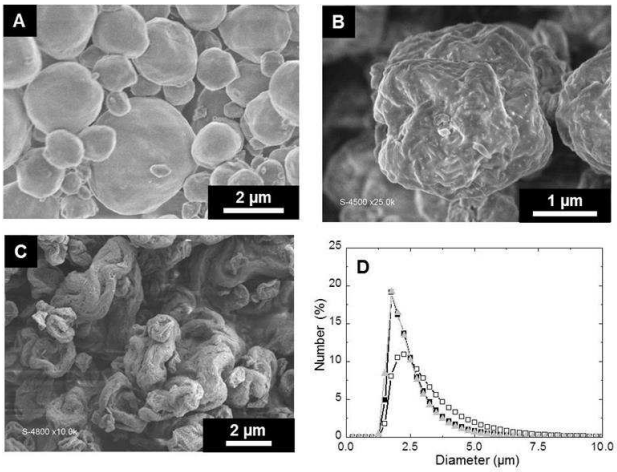

Fig. 2. (a) Nitrogen sorption isotherms at 77 K. (Symbols ■, ●, ▲, ▼ and ◊ correspond to calcined materials synthesized with ϕ_{CHI} = 0.15, 0.25, 0.33, 0.5 and 0.65, respectively). (b) Porous volume fraction as function of chitin volume fraction. (c) Porous volume fraction as function of surface area. The lines are only guides to the eye.

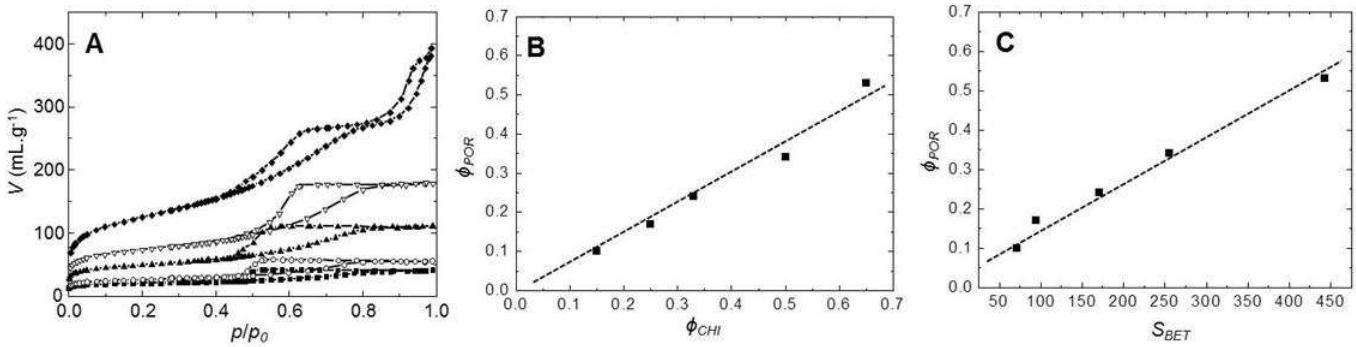

Fig. 3. Mercury porosimetry of SiO_2/TiO_2-A obtained with ϕ_{CHI} = 0.65 and Si/Ti =19.

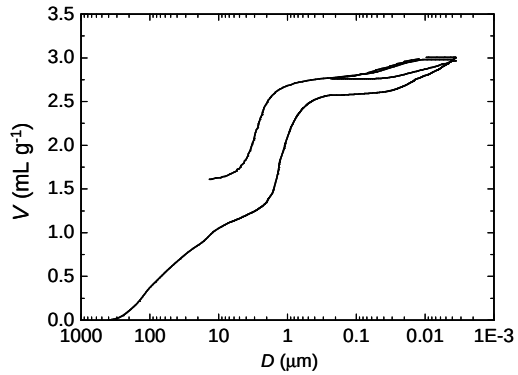

Fig. 4. TEM images of SiO_2/TiO_2-A materials (Si/Ti = 19) with ϕ_{CHI} = 0.15 (a, d), 0.33 (b, e), 0.65 (c, f) and corresponding schemes for materials synthesized with ϕ_{CHI} = 0.15 (g), 0.33 (h), 0.65 (j).

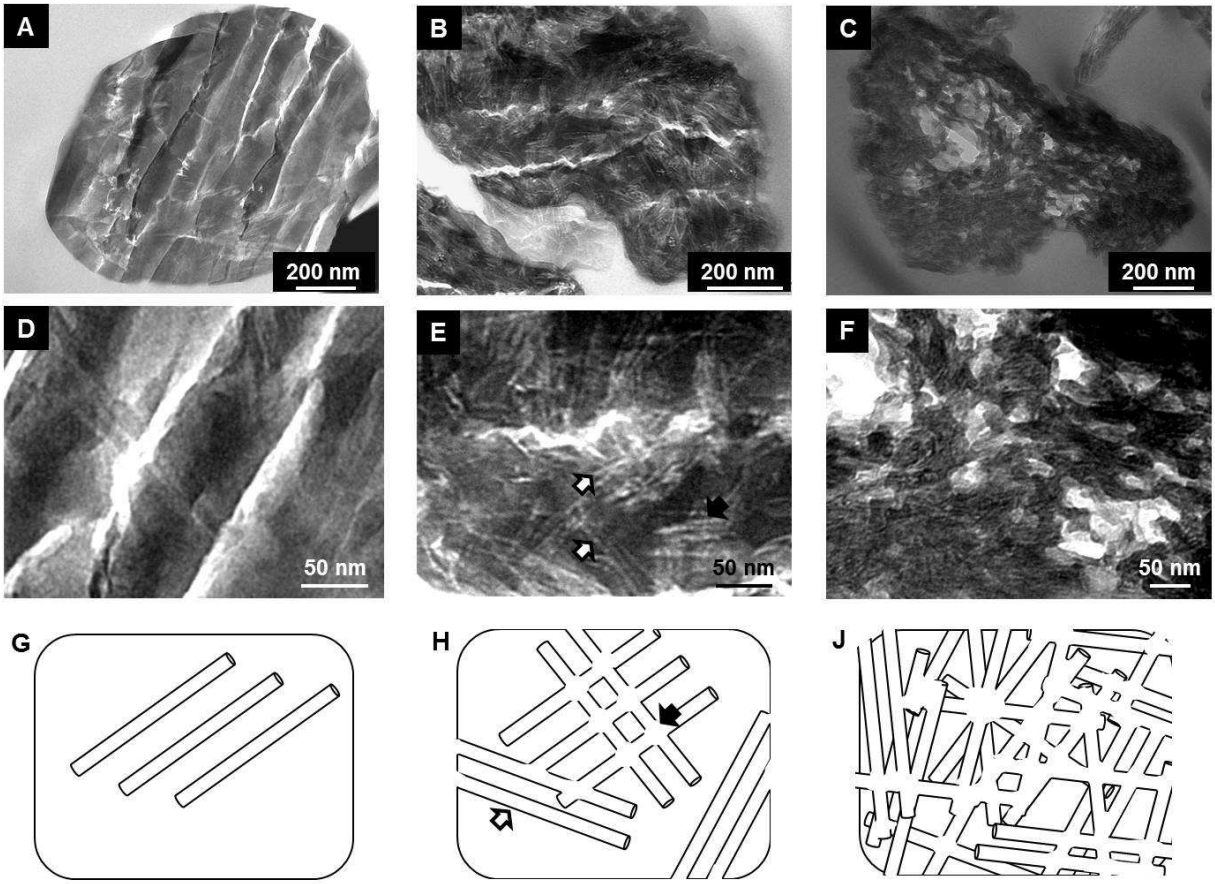

Fig. 5. High-resolution Ti2p-photoelectron spectra of calcined SiO_2/TiO_2-A sample with Si/Ti = 19 and ϕ_{CHI} = 0.65 (a), TS-1 (b) and anatase (c). Diffuse reflectance UV-Vis spectra of SiO_2/TiO_2-A sample with Si/Ti = 19 and ϕ_{CHI} = 0.65 (d), TS-1 (e) and anatase (f).

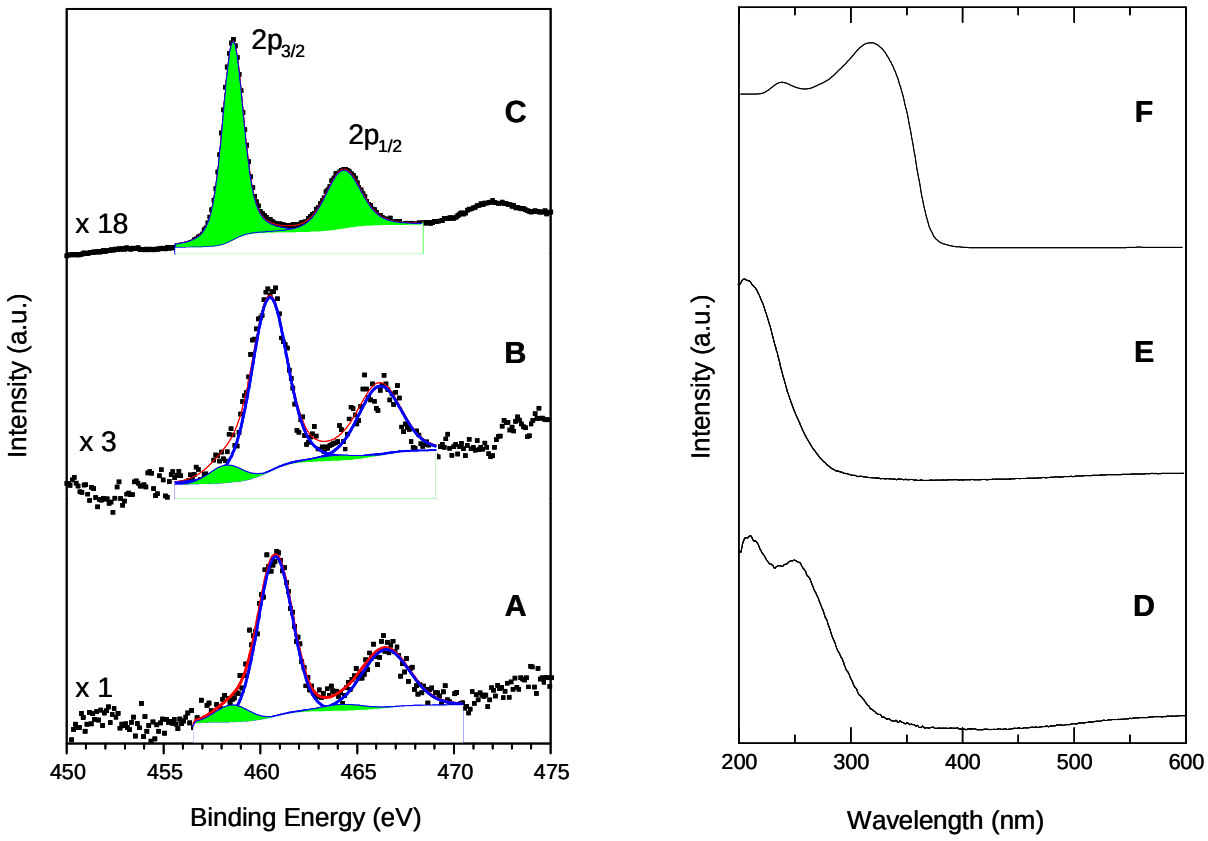

Fig. 6. Nitrogen sorption isotherms at 77 K for SiO_2/TiO_2-A (black) and -C (gray) samples synthesized with ϕ_{CHI} = 0.15 (a), 0.33 (b) and 0.65 (c) for Si/Ti = 19.

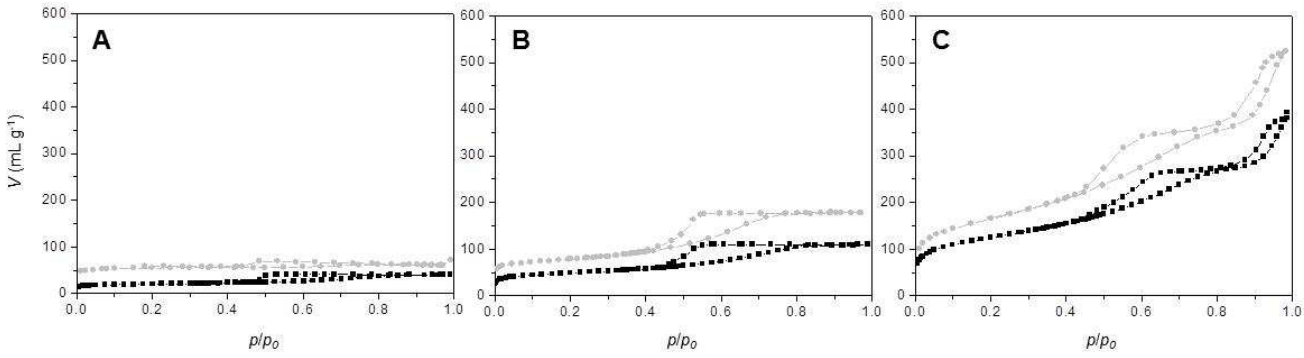

Fig. 7. Pore volume fraction as function of chitin volume fraction ϕ_{CHI} for SiO_2/TiO_2-A (▲) and SiO_2/TiO_2-C (■) for Si/Ti = 19.

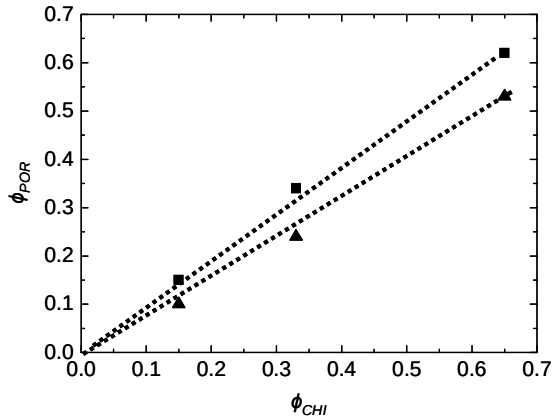

Fig. 8. Conversion of MPS (a) and DBT (b) as function of time (catalyst SiO_2/TiO_2-A with Si/Ti = 19 and ϕ_{POR} = 0.53). Gray: Mono-oxidized product. Black: di-oxidized product.

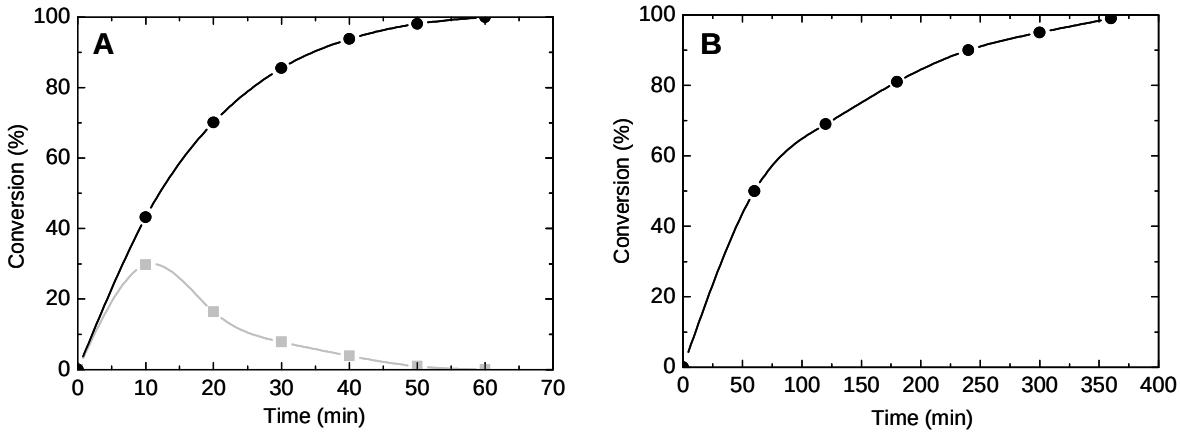

Fig. 9. Initial reaction rate (a), productivity after 30 min (b) and initial reaction rate averaged over specific surface area (c) as function of initial chitin volume fraction ϕ_{CHI} (Si/Ti = 19).

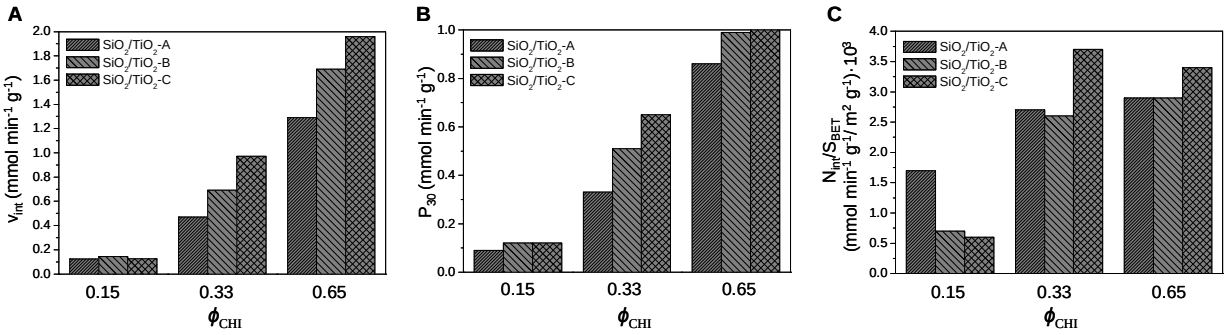

Fig. 10. (a) Recycling of catalysts, ■: SiO_2/TiO_2–A, ●: SiO_2/TiO_2–B and □: SiO_2/TiO_2–C (ϕ_{CHI} = 0.33, Si/Ti = 19). (b) Diffuse reflectance UV-Vis spectra of SiO_2/TiO_2-A sample, before (black line) and after (gray line) reaction.